Low-frequency radio emission in the massive galaxy cluster MACS J0717.5 + 3745

M. Pandey-Pommier, J. Richard, F. Combes, K. S. Dwarakanath, B. Guiderdoni, C. Ferrari, S. Sirothia, D. Narasimha

Low frequency radio emission in the massive galaxy cluster MACS *J*0717.5 + 3745

M. Pandey−Pommier[1], J. Richard[1], F. Combes[2], K. S. Dwarakanath[3], B. Guiderdoni[1], C. Ferrari[4] S. Sirothia[5] and D. Narasimha[6] ⋆

[1] Université de Lyon, Lyon, F-69003, France ; Université Lyon 1, Observatoire de Lyon, 9 avenue Charles André, Saint-Genis Laval, F-69230, France ; CNRS, UMR 5574, Centre de Recherche Astrophysique de Lyon ; Ecole Normale Supérieure de Lyon, Lyon, F-69007, France
[2] LERMA, Observatoire de Paris, 61 avenue de l'Observatoire, 75014 Paris, France
[3] Raman Research Institute, Bangalore 560 080, India
[4] Laboratoire Lagrange, UMR7293, Université de Nice Sophia-Antipolis, CNRS, Observatoire de la Cote d'Azur, 06300 Nice, France
[5] National Centre for Radio Astrophysics, TIFR, Pune University Campus, Post Bag 3, Pune 411007, India
[6] Theoretical Astrophysics Group, Tata Institute of Fundamental Research, Homi Bhabha Road, Bombay 400 005, India

Received ; accepted

ABSTRACT

Context. To investigate the non−thermal emission mechanism and their interaction during cluster mergers we analyze multiple low−frequency radio data for the $X - ray$ luminous massive galaxy cluster MACS J0717.5 + 3745, located at $z = 0.5548$. Large scale structure formation models in the Universe suggest that, galaxy clusters grow via constant accretion of gas, merger of galaxy groups and smaller clusters. Low Frequency radio observations trace such mergers in the form of relics and halos.
Aims. The dual frequency observations were performed on MACS J0717.5 + 3745 to investigate the spectral index pattern of the non−thermal emission and its interaction within the Intra Cluster Medium (ICM), during merger process.
Methods. Continuum observations were carried out using GMRT at 0.235 and 0.61 GHz on MACS J0717.5 + 3745 and archival data from the VLA (0.074 and 1.42 GHz) and WSRT (0.325 GHz) was used to complement the results. Furthermore, to explore the thermal and non−thermal interactions within the ICM and the morphological distribution, *Chandra* X−ray and *HST* data were used.
Results. Highly complex non−thermal radio emission distribution is seen in the cluster, at very low frequencies, with a global spectral index, $\alpha_{0.61}^{0.235} =\sim -1.17 \pm 0.37$. We have detected a giant radio halo within the cluster system with a linear size of 1.58 Mpc and a '*Chair − shaped*' filament structure between the merging subclusters of linear size 853 kpc at 0.235 GHz. This is the most powerful halo ever observed with $P_{1.4} = 9.88 \times 10^{-25} WHz^{-1}$ and an equipartition magnetic field estimate of $\sim 6.49\mu$G. The bright filament structure is well located in the central merging region of subclusters with enhanced temperature, as shown by *Chandra* and *HST* data analysis, further indicating the formation of this structure due to shock waves encountered within the ICM during the merger events.

Key words. Cosmology: large−scale structures of Universe− galaxies: clusters: individual: MACS J0717.5 + 3745− radiation mechanisms:non−thermal

1. Introduction

Cluster of galaxies are the largest gravitationally bound systems in the Universe. They are formed by mergers of smaller clusters and galaxy groups, as well as through continuous accretion of gas. Within the cluster, dark matter represents $\sim 80\%$ of the gravitating matter followed by $\sim 15\%$ of diffuse hot gas and $\sim 5\%$ is in luminous matter within the galaxies and the embedding Intra Cluster Medium, (ICM) (Feretti et al. 2012). Important progress in the study of ICM and their interactions in galaxy clusters have been made with multi−wavelength observations (Boselli & Gavazzi 2006; Markevitch & Vikhlinin 2007), however, less is known about the physical properties and the origin of non−thermal diffuse intra cluster components, that also play a vital role in the evolution of galaxy clusters (Dursi & Pfrommer 2008; Parrish et al. 2009) and constrain the large−scale structure formation scenario.

In fact, deep radio observations showed that in some clusters significant diffuse synchrotron emission is present, that indicate the existence of magnetic fields and cosmic rays within the cluster volume (Ferretti et al. 2005a, Ferrari et al. 2008, Kale & Dwarakanath 2009). These diffuse radio sources of different size scales (100 kpc to >Mpc) with surface brightness down to 0.1μJy $arcsec^{-2}$ at 1.4 GHz are known in about 80 clusters to date, at different cluster locations (center, intermediate, periphery) (Feretti et al. 2012, van Weeren et al. 2010). They are further classified as relics, mini−halos, and halos. They are steep−spectrum ($S(\nu) \propto \nu^{-\alpha}, \alpha > 1$) sources and represent the best evidence for the presence of large−scale magnetic fields and relativistic particles at different cluster locations (relics at the periphery, Giovannini & Feretti 2004; Bonafede et al. 2009a, mini−halos in the central regions of relaxed clusters, Govoni et al. 2009, Murgia et al. 2010, and halos in non relaxed clusters, Feretti & Giovannini 2008).

Observational and theoretical evidence are favoring the hypothesis that the origin of relativistic particles in clusters is related to merging events (so called electron primary model accel-

Table 1. GMRT observations and data from archive

Observation	$VLSS^a$	$GMRT^b$	$WSRT^c$	GMRT	$NVSS^d$	$FIRST^e$
Frequency (MHz)	74	235	325	610	1420	1420
Bandwidth (MHz)	1.56	2×16	120	2×16	2×50	50
Channel width	122 KHz	125 kHz	5 MHz	125 kHz	50 MHz	3 MHz
Observation dates	Archive	5 Nov, 2012	Archive	5 Nov, 2012	Archive	Archive
Total on−source time (hrs)	−	~4.5	−	~4.5	−	−
Synthesized beam (arcsec)	80×80	13×11	54×54cosecδ	5.7×4.8	45×45	5×5
rms noise, $\sigma(mJy\ beam^{-1})$	73	0.65	3.1	0.048	0.42	15

Notes. a−Cohen et al. 2007, b−23rd cycle observations, c−Rengelink et al. 1997, d−Condon et al. 1998, e−Becker et al. 1995

eration). There are several observational probes that agree with primary model predictions. In particular, Mpc scale radio halos have been detected only in merging clusters, showing a correlation between radio and X−ray luminosity, and, in a few cases, a spectral steepening as a function of frequency and distance from the cluster center (e.g. Giovannini et al. 2009; Venturi et al. 2007, 2008; Brunetti et al. 2008). The radio halo emission is centrally situated and typically unpolarized (except A2255, Govoni et al. 2005 and MACS $J0717.5 + 3745$, Bonafede et. al. 2009b). Further, radio halos are expected to result from electron acceleration due to intracluster turbulence (Brunetti et al. 2001; Petrosian 2001). On the other hand, radio relics are bright elongated or round structures (Feretti et al. 2012) situated at the peripheral regions with variable sizes up to megaparsecs scale. Electrons in radio relics are expected to be accelerated through diffusive shock acceleration (DSA), related to shock waves resulting from merging or accretion shocks in clusters (e.g. Ferrari et al. 2008). Relics are highly polarized (~ 20 − 30%) and irregular in nature with mostly steep spectrum ($\alpha \geq 1$) (Drury 1983; Ensslin et al. 1998; Finoguenov et al. 2010; Miniati et al. 2001; Bruggen et al. 2011). A magnetic field of μG level has been detected in radio relics with relativistic particles in cluster outskirts. Furthermore, there are 42 halos currently known, where 39 clusters show at least 1 or more relic source (for a total of 50 relics) (Feretti et al. 2012, Bagchi 2003).

MACS $J0717.5 + 3745$ is a massive X−ray luminous merging cluster, $L_X = (24.6 \pm 0.3) \times 10^{44} ergs^{-1}$ with ICM temperature 11.6 ± 0.5 keV located at $z = 0.5548$, discovered in the Massive Cluster Survey (MACS; Ebeling et al. 2001; Edge et al. 2003; Ebeling et al. 2007). It has a very complex morphological distribution showing multiple mergers with shock regions, known at high redshift and hence serves as a most promising target for studies of physical mechanisms driving merger events. Ebeling et al. 2004 discovered a 6−Mpc filamentary substructure leading into the cluster from south−east with optical observations from Subaru 8 m telescope. Ma et al. (2008 and 2009) presented optical ($HubbleS paceT elescope$ (HST), ACS; Keck−II, DEIMOS) and X−ray (*Chandra*) observations, and identified four distinct components in MACS $J0717.5 + 3745$ undergoing a triple merger event, instead of typically seen two cluster mergers e.g. $1ES 0657 − 56$ (Markevitch et al. 2002). Ma et al. analysed the galaxy and gas distribution with radial velocity informations and derived that the merger events may have formed the large−scale filament to the south−east of the cluster. Further, the ongoing merger give rise to shock heating which inturn increases the ICM temperature as measured in X−ray (*Chandra*) observations. The contiguous accretion of gas along the cluster−filament interface may give rise to large size (~ 1 Mpc) of the high temperature ICM region, as measured in MACS $J0717.5 + 3745$ X−ray observations. The clus-

ter is known to have disturbed morphological distribution with the largest Einstein radius, $\theta_e \sim 55''$ and shallow surface mass distribution (Zitrin et al. 2009). In strong lensing analysis studies four mass peaks were located in agreement with optically identified regions by Ma et al. 2008 and 2009 (Limousin et al. 2012). The Sunyaev−Zel′dovich effect (SZE) studies on the cluster was performed by Mroczkowski et al. 2012 with MUSTANG bolometer array on the Green Bank Telescope (GBT) between 90 − 268 GHz. The MUSTANG SZE data confirm that a pressure enhancement is seen in the shock-heated gas (≥ 20 keV) immediately adjacent to the extended radio emission as seen in low−frequency radio maps of this cluster and as previously indicated from Chandra observations.

The radio observations on the cluster have been equally interesting with the discovery of relic structure by (Edge et al. 2003), from the Faint Images of the Radio Sky (*FIRST*) at 20 cm (Becker et al. 1995) with no radio halo structure found in the data. Bonafede et al. 2009b conducted multi−frequency and multi−channel Very Large Array (VLA) observations at frequencies spanning $1.365−4.885$ GHz to further probe the cluster morphology and discovered a giant radio halo of 1 Mpc at 4.885 GHz and 1.5 Mpc at 1.365 GHz along with the 20% polarized radio substructure. The lack of Faraday rotation in the observations is not consistent with the assumption of relic produced by a merger shock near the center of the cluster. Further, no steepening of the spectral index across the short axis of the substructure is seen, as would be expected of a radio relic following a merger. Bonafede et al. thus argue that the substructure is not a radio relic, but rather a bright, polarized filament connected with the radio halo. A global spectral index for the entire diffuse radio emission of $\alpha_{4.9GHz}^{1.42GHz} = -1.27 \pm 0.02$ with an equipartition magnetic field estimate of $\sim 1.2\mu$G was derived assuming Jaffe−Perola emission model for the integrated radio spectra of the cluster (Jaffe & Perola 1973). van Weeren et al. 2009 further conducted GMRT observations at 0.614 GHz to study the diffuse radio emission within the cluster and found a radio relic of 700 kpc and giant radio halo of 1.2 Mpc with global spectral index of, $\alpha_{4.9GHz}^{0.61GHz} = -1.24 \pm 0.05$. The equipartition magnetic field of 5.8 μG was derived at the location of the radio halo from these observations. According to van Weeren et al. 2009, during the merger events the electrons within the cluster that are accelerated by Diffuse Shock Acceleration mechanism have formed the bright central radio substructure. However, the spectral index over the bright substructure varies roughly between −0.8 and −1.5, thus does not fit with merger shock scenario. In fact the Mach number values calculated using the spectral index information lies between 1.7 to 2.8, indicating relic might rather trace an accretion shock. Further, the high temperature regions of the ICM is co-spatial with the bright central radio substructure that is perpendicular to the merger axes of the cluster and large−scale filament, that
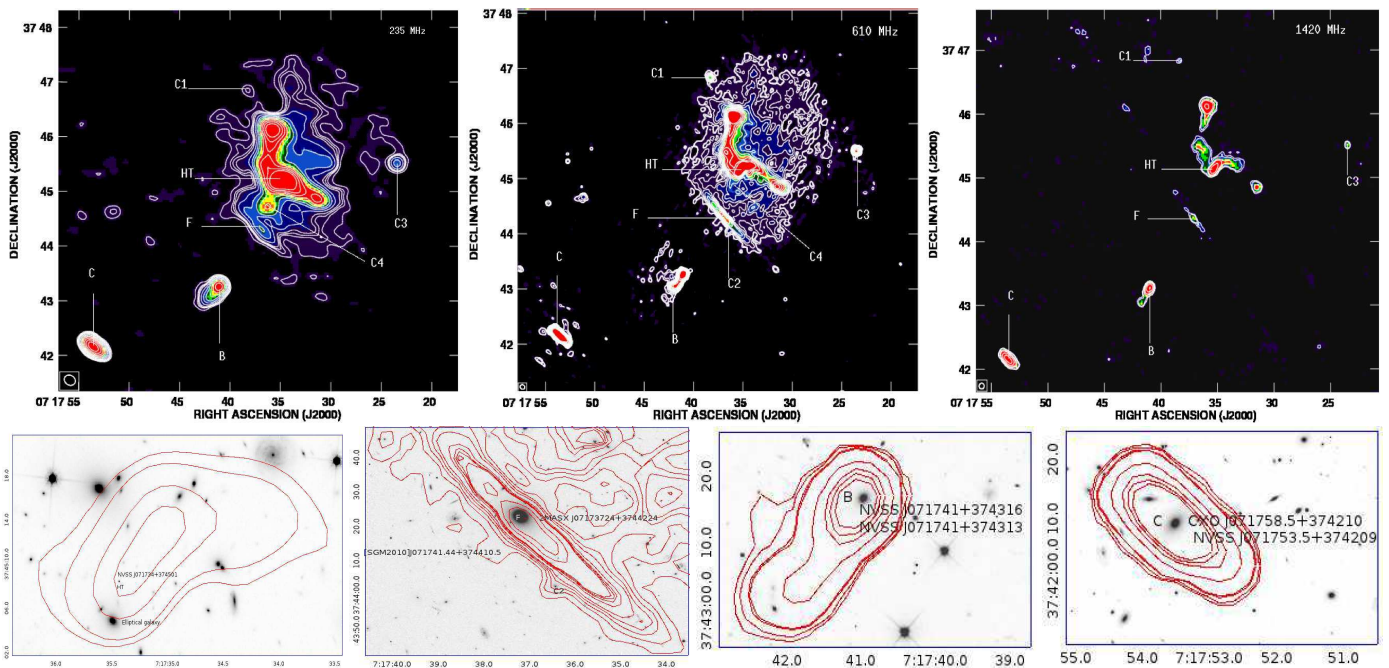
Fig. 1. High resolution radio images of massive galaxy cluster *MAS CJ*0717.5 + 3745 (*z* = 0.5548) at 0.235 GHz (*Top left*) at FWHM beam of 13.46″ × 10.76″ resolution, 0.61 GHz (*Top middle*) at FWHM of 5.70″ × 4.82″ resolution and 1.42 GHz (*Top right*) at FWHM of 5″ × 5″ resolution. Contours start at (3σ) and scale by a factor of $\sqrt{2}$. *Bottom panels:* Finding charts from HST for source HT, F (*z* = 0.1546), B and C with overlaid 0.61 GHz radio contours.

doesnot rules out the possibility that the relic might trace the merger shock scenario either. However such merger shocks are seen in clusters typically with radii less than 1 Mpc, contrary to MACS *J*0717.5 + 3745 where a cluster radii of greater than 1 Mpc is measured (Bonafede et al. 2009, van Weeren et al. 2009). Feretti et. al. 2012 have carried out a statistical study of diffuse radio emission in galaxy clusters and have not classified the bright central radio substructure as a '*relic*' due to its location in the cluster central region.

The main interest of our study for radio emission arising from galaxy clusters and ICM is to explore their spectral nature at very low frequencies (down to 0.235 GHz). With the high sensitivity data at 0.235 GHz we aim to get better estimates of luminosity and magnetic field, one of the fundamental ingredients in the physics of the ICM. By combining multi−frequency radio, *Chandra* and *HST* archival data it is possible to derive important correlations between shock regions and non thermal emissions. Ferreti et al. 2012, Murgia et al. 2010, studied the link between the cluster X−ray properties, their evolutionary stage and their non−thermal emission. These studies have been crucial for a comprehensive physical description of the intracluster medium and suggests that non−thermal emission play an important role in the cluster formation and evolution.

In this paper we present 0.235 and 0.61 GHz continuum observations of MACS *J*0717.5 + 3745 with the Giant Metre-wave Radio Telescope (GMRT). These observations are complemented by VLA and Westerbork Synthesis Radio Telescope (WSRT) archival observations. In Sect. 2 we give a brief overview of radio observations and data reduction. In Sect. 3, the radio images, spectral index maps, and spectra of discrete field sources are presented. Finally the discussion and conclusions are presented in Sects. 4 and 5. Throughout this paper we assume a ΛCDM cosmology with $H_0 = 71 km s^{-1} Mpc^{-1}$, Ω_M = 0.3, and Ω_Λ = 0.7. At the distance of MACS *J*0717.5+3745 (*z* =

0.5548), 1″ corresponds to 6.348 kpc (*www.astro.ucla.edu/ ∼ wright/CosmoCalc.html*).

2. Observation and data reduction

We have observed the massive cluster MACS *J*0717.5 + 3745 in the 23rd observation cycle using the GMRT at 0.235, and 0.61 GHz. The antennas were pointed at $RA = 07^h 17^m 32.63^s$ and $Dec = +37°44'59.70''$ (J2000). The visibilities were acquired at 128 spectral channels in continuum mode, in order to have better signal to noise ratio (S/N) and thus reduce the narrow band radio frequency interferences (RFIs). The details of the observations are summarized in Table 1, where we provide the frequency, total bandwidth, observation date, total time on source, beamwidth (FWHM) of the full array, and rms level (1σ) in the full resolution images. The visibility data was processed (calibration, flagging, imaging) with the NRAO's Astronomical Image Processing System (AIPS) software.

2.1. GMRT observations at 0.235 and 0.614 GHz

The 0.235 and 0.614 GHz observations consist of one data set each of 5.0h on source, collected on 5 November 2012. The observations were performed for both the Lower Side Band (LSB) and the Upper Side Band (USB) with a total bandwidth of 32 MHz splitted into 128 channels at 0.61 GHz and 8 MHz splitted into 60 channels at 0.235 GHz. The flux density scale was calibrated by the primary calibrators 3C 147 and 3C 286. The source 0735 + 331 was observed for 6 mins scan at intervals of ∼50 min and used as secondary phase and gain calibrator. The bandpass was calibrated using the sources 3C 286 and 3C 147. About 26% of the dataset that was affected by RFIs was flagged using task FLAGIT. Both data sets were averaged in frequency to eight channels to reduce bandwidth smearing effect and facilitate RFI flagging. Several cycles of imaging and phase
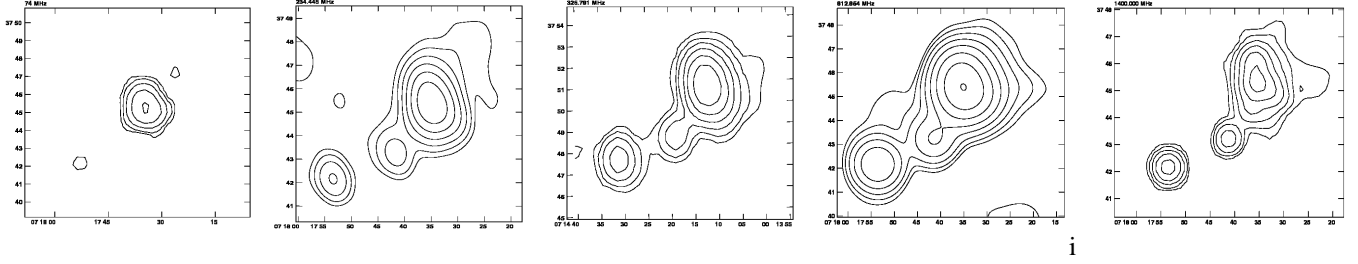
Fig. 2. Low resolution radio images of massive galaxy cluster *MAS C J*0717.5 + 3745 with contours starting at (3σ) and scaling by a factor of 2. *Left to right:* 0.074 GHz (VLSS; σ =73 mJy/beam; resolution = 80" × 80"), 0.234 GHz (GMRT; σ = 5mJy/beam; with resolution similar to WSRT), 0.325 GHz (WSRT, σ = 3 mJy/beam; resolution = 54"×84"; Coordinates in the map at BJ1950), 0.612 GHz (GMRT, σ = 0.69 mJy/beam; with resolution similar to WSRT), 1.400 GHz (VLA; σ = 0.41mJy/beam; resolution = 45" × 45").

self−calibration was applied to the data to produce initial phase corrected images. A final amplitude and phase self−calibration run was performed to obtain the final amplitude and phase corrected images. At 0.61 GHz both the IFs were simultaneously gridded, flagged, cleaned and imaged, while at 0.235 GHz only one IF was available for imaging. To minimize the effects of non-coplanar baselines while imaging in AIPS the polyhedron method (Perley 1989; Cornwell & Perley 1992) was used. To remove the sidelobes effect from the bright sources away from the field center, image size of twice the primary beam radius was cleaned using 3D-technique with multiple facets to account for the non-coplanarity of the incoming wavefront within the large primary beam. Natural weighting was applied to each dataset using robust parameter 0.5 (Briggs 1995), in order to give constant weights to all visibilities and pick up the diffuse structure. The contour levels of the full resolution 0.235 and 0.614 GHz image are shown in the Fig. 1. The radio image at 0.614 GHz has a FWHM beam of 5.70″ × 4.82″ and a noise level of 0.048 mJy/beam (1σ) and at 0.235 GHz has a FWHM beam of 13.46″ × 10.76″ and a noise level of 0.65 mJy/beam (1σ). Fig. 1 also shows the high resolution VLA map at 1.4 GHz obtained from the *FIRST* survey archive (Becker et al. 1994), with resolution similar to 0.61 GHz map. We have labeled the brightest radio sources close to the diffuse emission, alphabetically in order to further clarify the discussion on the association of these sources with the halo (ref. Fig. 1).

The theoretical noise in the image is given by

$$\sigma_{thermal} = \frac{\sqrt{2}T_{sys}}{G\sqrt{n(n-1)N_{IF}\Delta\nu t_{int}}} \quad (1)$$

where T_{sys}, the system temperature for GMRT = 92 K at 0.61 GHz and 177 K at 0.235 GHz. N_{IF}, the number of side bands recording both RR and LL polarizations = 1 at 0.61 GHz and 0.5 at 0.235 GHz. $\Delta\nu$, the bandwidth per sideband = 13.5 MHz at 0.61 GHz and 6.9 MHz at 0.235 GHz. n is the number of working antennas = 27 at both the frequencies. G is the antenna gain = $0.32KJy^{-1}$ at 0.61 GHz and $0.33KJy^{-1}$ at 0.235 GHz. t_{int} is the net integration time = 5 hours on the target source. The expected theoretical thermal noise at 0.61 GHz is typically 31μJy and at 0.235 GHz is typically 115μJy. The noise recorded in our maps are 48μJy at 0.61 GHz and 650μJy at 0.235 GHz. Due to natural weighting applied to the data during imaging, a increase in the recorded noise level by typically 10% as compared to the theoretical noise is seen. Further, at 0.235 GHz a significant increase in the sky temperature and RFI is seen that leads to increase in the noise by a factor of ~5.6 than the expected noise.

2.2. Archive data from VLA and WSRT

To investigate the multi−frequency extended radio emission from MACS *J*0717.5 + 3745 we have used the archival low resolution data available from the WENSS survey (Rengelink et al. 1997) at 0.325 GHz, the VLA at 0.074 GHz- the VLSS survey (Cohen et al. 2007) and 1.4 GHz VLA's NVSS survey (Condon et al. 1998). The details of the survey parameters are listed in table 1. The degraded resolution maps at lower frequencies increases the sensitivity to completely measure the arcmin size diffuse structure emission that lies completely within the primary beam. Fig. 2 shows the diffuse radio emission at various frequencies from MACS *J*0717.5 + 3745. The GMRT images at 0.235 and 0.614 GHz are convolved with poorer beam resolution in order to produce low resolution map comparable with 0.325 MHz map.

3. Results: Optical and radio properties- images and spectral analysis

We analyze the results of the GMRT observations with particular emphasis on the study of diffuse emission in our high sensitivity maps at 0.61 GHz and new image at 0.235 GHz. These observation will help us in determination of the total integrated radio spectrum down to 0.235 GHz for the cluster halo, bright central filament structure and discrete field sources (HT, F, B, C, C1, C2, C3 and C4, ref. Fig. 1) that are related to the cluster and the large−scale optical and X−ray filaments. The new 0.235 GHz map allows us to derive much better the spectral index, and therefore the various probable (re−)acceleration mechanisms, as steep spectra index implies aged radio plasma, with no recent re−acceleration activity. Furthermore, the low frequency image at 0.235 and 0.61 GHz allows us to explore the nature of two new contaminating steep spectrum field sources (C2 and C4) within the halo, that are often not detected at higher frequencies. These compact sources donot contribute into diffuse emission from the halo and have different origin, hence they were subtracted from the data during the flux density measurements. The flux density of radio halo, bright central filament structure and field sources (HT, B and F) at the different frequencies has been determined by using AIPS task IMSTAT, due to their extended nature. The task JMFIT was used to determine the flux density of unresolved sources (C, C1, C2, C3 and C4). We determined the flux density by integrating their radio brightness down to the 3σ level.

3.1. The '*Chair − shaped*' filament structure

The high resolution images at 0.61 GHz and 0.235 GHz (Fig. 1) reveal a bright elongated substructure or '*Chair − shaped*'

Table 2. Integrated spectra for cluster and '*Chair − shaped*′ filament structure

Source	Beam ″×″	ν (GHz)	Flux density (mJy)	Size (Mpc)
Relic	18×14	4.8	16.00*	-
	5×4	1.42	83.00*	0.83
	5.70×4.82	0.61	260±3	(1.9′=)0.772
	84×54	0.325	-	-
	13.46×10.76	0.235	844±8	(2.1′=)0.853
	80×80	0.074	-	-
Halo	18×14	4.8	26±1*	1
	21×18	1.42	118±5*	1.5
	13.34×11.05	0.61	162±0.23	(3.7′=)1.5
	84×54	0.325	1200±0.5*	1.8
	25.45×22.31	0.235	492.5±0.52	(3.9′=)1.58
	80×80	0.074	5800±0.6	1.3

Notes. * Bonafede et al. 2009b

filament that was discovered by Edge et al. 2003 as the '*relic*′ within the cluster. This bright elongated substructure runs from north to south with a twist towards south−west. At the north, center and south end of this structure enhanced radio emission is measured. The linear size of the entire structure is 853 kpc at 0.235 GHz and 772 kpc at 0.61 GHz in GMRT maps. We have provided better size estimates (about ∼70 kpc more) with our maps as compared to van Weeren et al. 2009 due to better sensitivity achieved in our observations. The *FIRST* survey map at 1.4 GHz shows the '*Chair − shaped*′ filament with a total linear size of 731 kpc. The physical properties of this bright central filament derived from high resolution maps are listed in table 2. In addition to the '*Chair − shaped*′ structure, Fig. 1 also shows the associated field source HT, located mid−way along the elongated central filament and its detection at optical wavelength. Source HT is identified as "*head − tail*" source from radio observation by van Weeren et al. 2009. We confirm with our observations the detection of the tail structure down to 0.235 GHz and steepening in the spectral index map (*Fig. 3*), as expected at lower frequencies. We have identified radio galaxy NVSS *J*071734 + 374501, from the Nasa/IPAC Extra−galactic Database (NED) as a likely counterpart for source HT. No optical counterpart was detected in DSS2−red map by Edge et al. 2003. However, the core of the radio galaxy was identified to be coincident with the optical counterpart in the *HST* image with a spectral index of ∼ 0.7 (Bonafede et al. 2009b). van Weeren et al. 2009 further identified an elliptical galaxy located within the cluster at RA 07^{h}17^{m}35^s.5, Dec +37°45′0.5″.5 as a likely counterpart. A steep spectral index of −1.55 was derived from low resolution image by van Weeren et al. 2009 indicating that the emission from the tail region is partially contaminated by the surrounding emission from the '*Chair − shaped*′ filament region. Further, the unresolved source C4 located mid−way below the '*Chair − shaped*′ structure is a new detection in our 0.235 GHz and not detected at 0.61 GHz. The source is associated to compact AGN from *NED* catalog and has highly steep spectrum with cut−off frequency at 0.61 GHz (*ref.Fig.3 Bottom Panel*) .

3.2. The extended radio halo

With the high sensitivity and better resolution observation performed with the GMRT at 0.61 and 0.235 GHz, we have managed to map the most distant halo within the galaxy cluster MACS *J*0717.5 + 3745 (*z* = 0.5548) down to 0.235 GHz. The diffuse extended radio halo emission is detected all around the bright central radio substructure with a total size of about 1.50 Mpc at 0.61 GHz and 1.58 Mpc at 0.235 GHz. As the noise is high in the FIRST survey data at 1.4 GHz(Fig. 1 *rightpanel*), the diffuse structure is not detected, though the resolution is similar to GMRT at 0.61 GHz. However, the NVSS low resolution map at 1.4 GHz (*Fig. 2 Panel 5*) shows a diffuse halo structure of roughly ∼4 arcmin (corresponding to a linear size of 1.58 Mpc), while the apparent angular extent of the halo in the WNESS image is ∼4.67 arcmin, corresponding to ∼1.8 Mpc (Bonafede et al. 2009b). Table 2. shows the physical properties of the halo structures at multi-frequency that are derived from lower resolution maps that allows best to extract the diffuse structure.

The low resolution maps in Fig. 2 shows the extended halo structure clearly detected at 0.074, 0.235, 0.325, 0.61 and 1.4 GHz with resolution (∼ 54″ × 84″) similar to WSRT at 0.325 GHz or poorer. The 0.61 GHz map has a very good sensitivity to the extended emission as compared to 0.235 GHz map due to reduced noise level of about 0.69 mJy/beam. At 0.074 GHz less diffuse structure is detected around the central halo due to poorer sensitivity of 73 mJy/beam, while at 1.4 GHz the diffuse structure is slightly resolved out due to better resolution as compared to WSRT map.

3.3. The discrete field sources

In addition to the '*Chair − shaped*′ filament, source HT, compact sources C4 and halo structure, Figure 1 and Table 3, also shows the associated field sources (C1, C2, C3, F, B, C) and their detection at optical wavelengths. An elongated source F is detected at the south−west edge of the halo, below the cluster center. This source is identified at redshift, *z* = 0.1546 (van Weeren et al. 2009), as FR−I type (Fanaroff & Riley 1974) source with compact core and diffuse linear extension (on both sides) of the order of ∼ 1′ from GMRT 0.61 GHz data (van Weeren et al. 2009). We have identified a radio galaxy, 2MASX *J*07173724+3744224, as a counterpart for source F from *NED* catalog. It is interesting to note that another radio galaxy [*SGM*2010]071741.44+374410.5 located at redshift, *z* = 0.55 is also identified in the radio map. We also confirm the identification of faint compact source C2 by van Weeren et al. 2009. This source is buried in the extended emission from source F and has AGN as counterparts. Two slightly resolved sources B and C are detected outside the halo in the south−west direction along the X−ray and optical large scale

Table 3. Integrated spectra for field sources

Source	RA DEC	ν (GHz)	Flux density (mJy)	morphology	Counterparts from *NED*	z
Source- HT	$07^h17^m32.64^s$ $37°44'59.66"$	4.8 1.42 0.61 0.325 0.235 0.074	3.9* 22.4* 109.8±3.2 - 573±7 -	*head − tail*	Elliptical galaxy NVSS J071734 + 374501	unknown unknown
Source- F	$07^h17^m36.86^s$ $37°44'19.66"$	4.8 1.42 0.61 0.325 0.235 0.074	- 9.08* 30.29±0.5 10.17* 63.17±3 219.24^a	core+lobes	2MASX J07173724 + 3744224	0.1546
Source- B	$07^h17^m41.07^s$ $37°43'14.65"$	4.8 1.42 0.61 0.325 0.235 0.074	6.40* 18.3* 44.79±2.6 61.22* 100.93±0.8 219.24^a	*head − tail*	NVSS J071741 + 374316 NVSS J071741 + 374313	unknown unknown
Source- C	$07^h17^m53.50^s$ $37°42'09.55"$	4.8 1.42 0.61 0.325 0.235 0.074	14.70* 32.30* 75.96±1 115.18* 109.75±0.6 219.24^a	unresolved	CXO J071753.5 + 374210 NVSS J071753.3 + 374209	unknown unknown
Source- C2	$07^h17^m36.37^s$ $37°44'03.37"$	4.8 1.42 0.61 0.325 0.235 0.074	- - 0.98±0.05 - 1.95±0.5^a -	unresolved		unknown
Source- C4	$07^h17^m36.26^s$ $37°44'43.80"$	4.8 1.42 0.61 0.325 0.235 0.074	- - 0.15±0.1^a - 29.64±0.7 -	unresolved		unknown

Notes. a = 3σ upper limit from the map, * Bonafede et al. 2009b

filament (Ebeling et al. 2004). Source B has a compact core with "*head − tail*" morphology and has two variable radio galaxies (NVSS *J*071741 + 374316, NVSS *J*071741 + 374313) identified as counterparts from the *NED* catalog. For the unresolved source C also two radio galaxies (CXO *J*071753.5 + 374210 and NVSS *J*071753.3 + 374209) are identified as *NED* counterparts. The main properties of the identified radio galaxies along with their position coordinates, flux densities, morphology and counterparts are listed in Table 3. We need to take into account the possible contamination from these radio galaxies embedded within the diffuse emission, in order to conduct a proper study of the diffuse emission associated with the ICM. The compact field sources (C1 and C3) are not listed in the table, as they dont show extended diffuse structures and hence donot contribute into the halo emission.

Furthermore, the low−resolution images (Fig. 2) reveal a bridge of diffuse radio emission, which connects the radio galaxies B and C with the cluster halo. This connecting diffuse radio emission bridge has an angular size of ∼ 9*arcmin*

which transforms to linear scale size of 3.66 Mpc and is coincident with the large−scale filament funneling matter onto MACS *J*0717.5 + 3745 that has been detected at optical and X-ray wavelengths by Ebeling et al. 2004 and Ma et al. 2009. This bridge emission is best detected at 5σ level in the 0.61 GHz low resolution map due to its high sensitivity and confirm the detection at 0.325 GHz by Bonafede et al. 2009b. At 0.234 GHz and 0.074 GHz, the bridge emission is partially detected as the noise is comparatively higher in the map. The faint bridge emission is not detected in higher resolution VLA map at 1.4 GHz as compared to 0.235, 0.325 and 0.61 GHz maps. The detection of radio emission in this area further indicates the presence of magnetic field initially within the filament before the amplification due to merger event. The diffuse bridge emission could also be a part of the whole diffuse halo structure; however, further observations at frequencies below 0.325 GHz with sensitivity below 0.69 *mJy/beam* are needed with radio facility like LOFAR in order to confirm this result and explain mechanism empowering relativistic electrons to emit at such large linear scales.
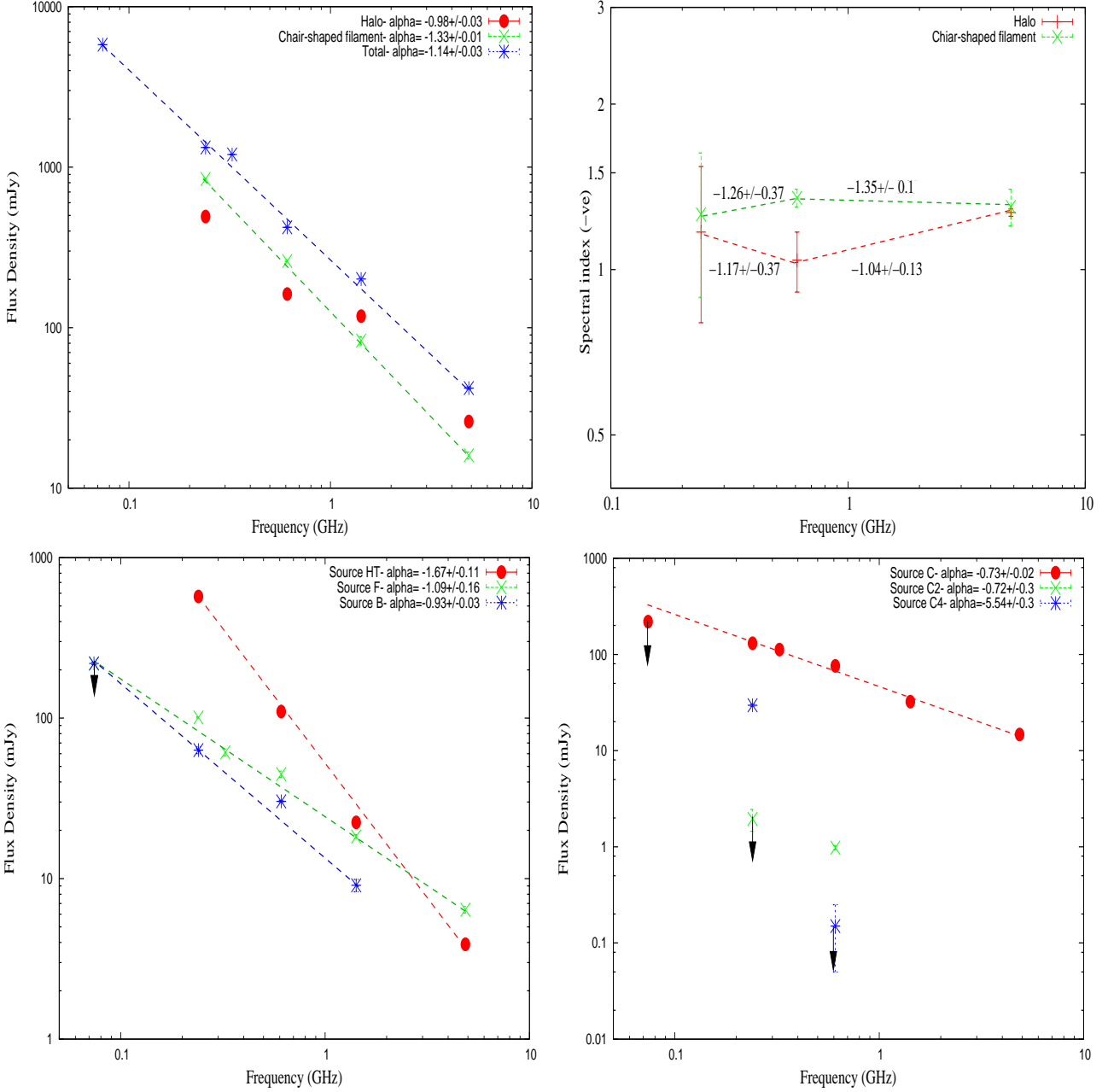
Fig. 3. *Top 1st panel:* Integrated radio spectra of the halo, '*Chair − shaped*' filament source and total(halo+'*Chair − shaped*' filament source). *Top 2nd panel:* spectral index variation with respect to frequency for the halo and '*Chair − shaped*' filament source. *Bottom 1st panel:* Integrated radio spectra of extended sources HT, B and F; *Bottom 2nd panel:* Integrated radio spectra of compact source C, C2 and C4. The down arrows represent the 3σ detection limit. Data from literature are plotted at 4.86, 1.4, 0.325 and 0.074 GHz along with 0.61 and 0.235 GHz GMRT data.

3.4. Integrated radio spectra for cluster and discrete sources

Radio spectra serves as an important tool for understanding the origin of the relativistic electrons emitting non−thermal emission in galaxy clusters. The non-thermal synchrotron emission detected in cluster of galaxies follow a typical power law decay with $S(\nu) \propto \nu^{-\alpha}$, where $S(\nu)$ is the flux density, ν is the frequency and α is the spectral index. To understand the connection between the halo and discrete field sources it is important to understand their spectral nature. We analyzed the integrated radio spectra of the '*Chair − shaped*' filament, halo and sources HT, B, C, C2, C4 and F by complementing the GMRT measurements at 0.235 and 0.614 GHz with the flux densities available in literature and archival data.

The integrated spectral index was computed using the relation

$$\frac{Log S(\nu)}{Log(\nu)} = \alpha \qquad (2)$$

A global spectral index of, $\alpha_{4.86}^{0.235} = -1.33 \pm 0.01$ was obtained for the '*Chair − shaped*' filament by excluding source HT and C4, between 0.235 and 4.86 GHz, from high resolution maps as shown in Fig. 3 and in agreement with Bonafede et al. 2009b. The error in the spectral index values is obtained from linear fit to the data over the frequency range 0.235 to 4.86 GHz. Overall, the GMRT measurements agree both with the adjacent data points taken from the literature and the straight line fit, thus providing a consistent check of the flux density scale in our im-

ages. The 'Chair – shaped' filament spectral index, $\alpha_{0.61}^{0.235} = -1.26 \pm 0.37$ and $\alpha_{4.86}^{1.4} = -1.35 \pm 0.1$ suggests steepening in the spectra at higher frequencies as compared to lower frequencies (*Fig.*3 *Top Panel*). In the case of radio halo, a global spectral index, $\alpha_{4.86}^{0.235} = -0.98 \pm 0.03$ was computed, from the lower resolution maps by excluding the source F, C2, C1, and C3. Bonafede et al. 2009b derived a spectral index, $\alpha_{4.86}^{1.42} = -1.27 \pm 0.02$, where as van Weeren et al. 2009 derived a value $\alpha_{4.86}^{0.61} = -1.24 \pm 0.05$. Further, van Weeren et al. 2009 computed a spectral index, $\alpha_{1.42}^{0.61} = -1.04 \pm 0.13$ and we have derived a spectral index, $\alpha_{0.61}^{0.235} = -1.17 \pm 0.37$ from our observations (*Fig.*3 *Top Panel*). The error in the spectral index value between 0.235 and 0.61 GHz was calculated using the noise in the image and flux density error measurements (Chandra et al. 2004). The analysis of spectral index suggests a steeping at higher frequencies due to spectral ageing that might lead to high frequency cut−off. Further, the steepness seen at lower frequencies could be due to more population of low energy emitting relativistic particles available within the cluster volume (van Weeren et al. 2012). The total flux of the radio halo at 0.61 GHz and 0.235 GHz are $\sim 162 \pm 0.23$ mJy and $\sim 492.5 \pm 0.52$ mJy respectively. Hence the monochromatic radio power at 1.42 GHz computed with $\alpha_{0.61}^{0.235} = -1.17$ is, $P_{1.42} = 9.88 \times 10^{25} W Hz^{-1}$. Thus, MACS J0717.7+3745 is one of the most powerful radio halo ever observed. The power estimate is slightly less then Bonafede et al. 2009b, as we have extrapolated the halo flux at 1.42 GHz using $\alpha_{0.61}^{0.235} = -1.17$ and might have missed some additional diffuse emission due to limited sensitivity for large angular scale. However, we have provided better flux and radio power estimates at 1.42 GHz as compared to van Weeren et al. 2009 due to our high sensitivity maps.

Important information about the magnetic field in this cluster can be derived from the spectral analysis performed above. The strength of the magnetic field can be estimated by assuming minimum energy densities in the radio sources. The minimum energy density (in units of erg/cm^3) is given by

$$U_{min} = \zeta(\alpha, \nu_1, \nu_2)(1 + k)^{4/7} \nu_0^{-4\alpha/7}(1 + z)^{(12-4\alpha)/7} I_0 d^{-4/7} \quad (3)$$

where $\zeta(\alpha, \nu_1, \nu_2)$, a constant tabulated in Govoni & Feretti 2004, is 2.29×10^{-13}, α is -1.17, I_0 the surface brightness is 7.78 $\mu Jy arcsec^{-2}$ at frequency $\nu_0 = 1420$ MHz, d the depth of the source is 1580 (kpc), and k the ratio of the energy in relativistic protons to that in electrons = 100. A volume filling factor of one has been assumed in the above equation. The equipartition magnetic field in terms of minimum energy is thus given as

$$B_{eq} = \sqrt{\left(\frac{24\pi}{7} U_{min}\right)} \quad (4)$$

Using the quantities above, we compute the minimum energy, $U_{min} = 10.87 \times 10^{-13}$ $ergs/sec^3$ and the equipartition magnetic field strength, $B_{eq} = 3.43\mu$Gauss. The value of magnetic field derived is slightly higher as compared to van Weeren et al. 2009 due to better flux and linear size of the halo derived in our observations down to 0.235 GHz. This equipartition magnetic field strength is calculated on a fixed range of frequency (10*MHz* − 10*GHz*), however the upper and lower frequency limits are dependent on the energy of the radiating electrons (Brunetti et al. 1997; Beck & Krause 2005). Hence, considering the low and high energy cut−offs for the particle distribution and taking into account $\gamma_{min} \leq \gamma_{max}$, the energy boundaries indicated by the Lorentz factor, the revised equipartition magnetic field strength (B'_{eq}) is

$$B'_{eq} \sim 1.1 \gamma_{min}^{\frac{1+2\alpha}{3-\alpha}} B_{eq}^{\frac{7}{2(3-\alpha)}} \quad (5)$$
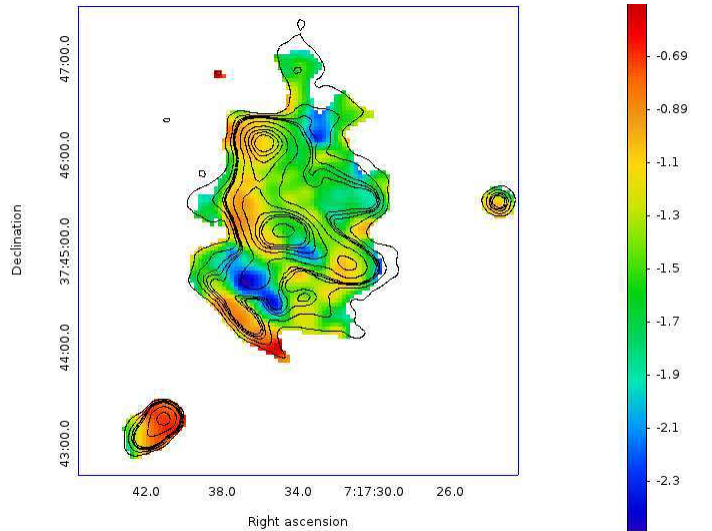
Fig. 4. Spectral index map between 0.235 and 0.61 GHz at a resolution of 13.3" × 10.7". Contours are from the 0.61 GHz image and drawn at a level of $[1, 2, 3, 4, 16, 32, ..] \times 0.15 mJy beam^{-1}$.

where, γ_{min} is 100. Thus the revised magnetic field strength, $B'_{eq} = 6.49\mu$gauss and two times larger than the standard equipartition estimate as expected (Govoni & Feretti 2004).

The main goal of this work is to constrain the spectral index of the halo in the MACS J0717.5 + 3745 cluster down to 0.235 GHz. Due to the faint and extended nature of the halo, it is complicated to derive such a constrain on the spectral index distribution. Using the best comparison between sensitivity and resolution in the 0.235 GHz image at a 13.46" × 10.76" resolution, we have created the spectral index map for the halo. In the Fig. 4 we present the spectral index image between 0.235 and 0.61 GHz with 0.235 GHz radio contours overlaid at a resolution of 13.3" × 10.7". The uncertainties in the computed
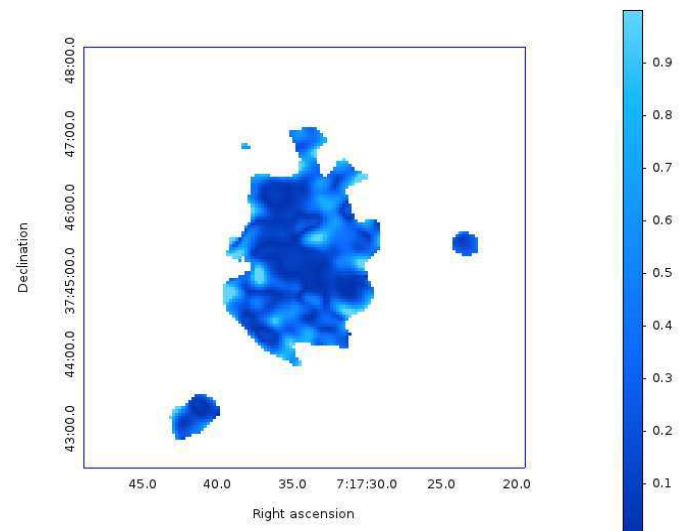

Fig. 5. Spectral index error map between 0.235 and 0.61 GHz image. The error map shows the uncertainties in the spectral index based on the rms noise in both the radio images.

spectral index map are also shown in Fig. 5 ranging from 0.09 to 0.9. The error in the spectral index estimate between 0.61 and 0.235 GHz as discussed earlier is consistent with the spec-
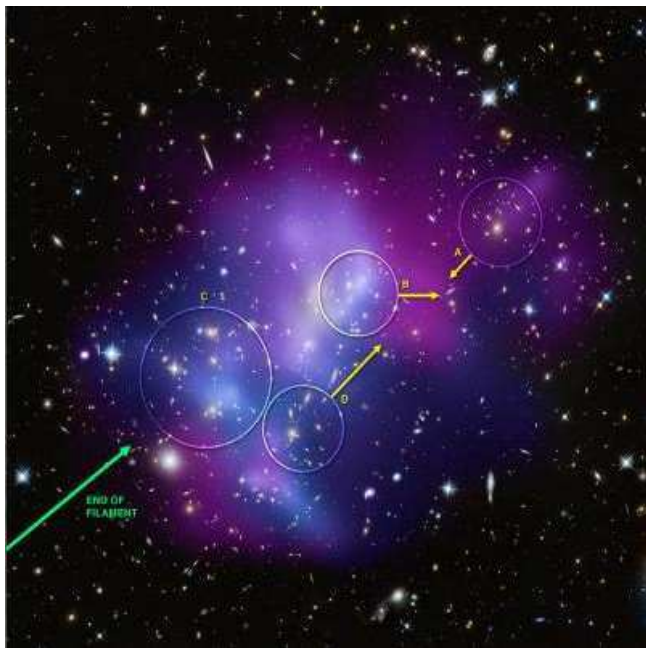
Fig. 6. MACS *J*0717.5 + 3745: Chandra colour image on HST showing galaxies in 4 different clusters involved in collision, with direction of motion for three fastest moving clusters. The length of the arrow shows the approximate speed in a direction perpendicular to the line of sight. The direction of motion of the cluster appears roughly parallel to the direction of the filament (Credit: X−ray (*NAS A/CXC/I f A/C.Maetal*.2008, 2009); Optical (*NAS A/S T S cI/I f A/C.Maetal*.2008, 2009)).

4. Discussion

Most galaxy clusters that host radio halos and bright filament also show signatures of recent or ongoing merger activities (Ferrari et al 2008). The massive cluster MACS *J*0717.5 + 3745 is a complex case involving triple merger (Ma et al. 2008, 2009). The implications to the spectral index trends in the diffuse radio emission in MACS *J*0717.5 + 3745 from the proposed origins in merger shocks is explored further here.

4.1. Cluster dynamics and ICM Temperature

A schematic representation of the Chandra map of MACS *J*0717.5 + 3745 (available from *NAS A/CXC/I f A/C*, Ma et al. 2008, 2009) is shown by the colored scale over HST map in (*Fig.6*), where the blue colour indicates the hottest region and reddish purple colour indicates the cooler region and the temperatures in between are represented by purple colour. (*Fig.7*) shows the radio contours overlaid on Chandra colour image. We have further identified 4 different regions of interest based on optical data, for further analysis within the halo marked as CL1, CL2, CL3, and CL4 shown in Fig. 7. The optical and X-ray studies (Ma et al. 2008, 2009) suggest that the cluster region marked as CL1 has already passed through the main cluster previously in the opposite direction and is likely falling back, whereas the cluster CL2 has unclear origin and has higher speed along the line of sight as compared to the other clusters. The cluster region labeled as CL3 is identified as the core of the main cluster based on the good alignment between the galaxies and hot gas for cluster CL3, along with its motion compared to MACS *J*0717.5 as a whole. While, region CL4 is a cooler (redder) region of gas and has likely survived from before the collision in the cluster. Further, CL1 and CL4 are also suggested to be originated from
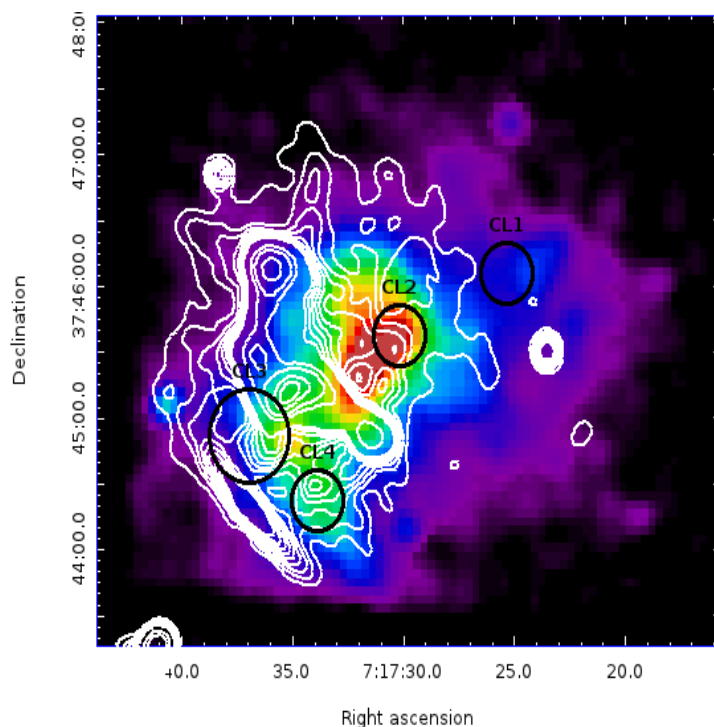
tral index error map. The spectral index is shown only in the regions where the flux is greater that 3σ at both the frequencies. Additional errors in the spectral index could be noticed due to different calibration errors and UV−coverage at both the frequencies. The overall radio spectrum of the halo is steep. The spectral index ranges from $\alpha \sim -0.85$, close to the cluster center, up to about $\alpha \sim -2.3$ at the edge. The analysis of the spectral index profile in the '*Chair − shaped*' filament structure shows a variation from -0.92 up to -1.5. The flatter spectral index in '*Chair − shaped*' filament is coincident with the high temperatures in merging region (Ma et al. 2008) and in agreement with the ICM temperature and flatness in the spectra correlation derived via Govoni et al. 2004. Source HT shows variation in spectral index from -0.95 near the head region to -1.8 towards the tail region. Such a spectral steepening from the head towards the lobes has been seen in radio galaxies and is believed to be due to spectral ageing due to synchrotron and Inverse Compton (IC) losses. As source HT has much steeper spectra as compared to the '*Chair − shaped*' filament, the radio emission from this region is expected to have different origin.

The extended sources F, B and C presents a power law radio spectrum with a spectral index of about $\alpha = -1.09 \pm 0.16$, $\alpha = -0.93 \pm 0.03$ and $\alpha = -0.73 \pm 0.02$ (*Fig.3 Bottom Panel*). This is a quite usual value for active radio galaxies. The study of the spectral index suggest that radio emission in these galaxies are less steeper as compared to that of the halo and the '*Chair − shaped*' filament structure and hence produced by different population of relativistic electrons.

Fig. 7. MACS *J*0717.5 + 3745: GMRT contours at 0.61 GHz overlaid on X−ray *Chandra* map with 4 different cluster regions involved in collision indicated by *circles*.
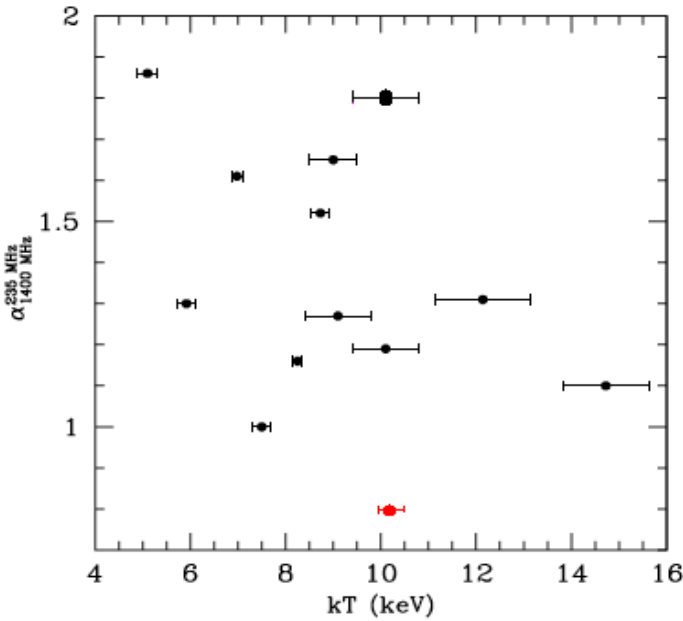
Fig. 8. Spectral index of radio halos in the 235 MHz-1.4 GHz interval as function of the cluster X-ray temperature (adapted from Venturi et al. 2013 and Giacintucci et al. 2013).The red points marks the position of MACS $J0717.5 + 3745$

the filament. The large region of relatively hot gas (shown in blue) is seen to extend from the left side of cluster CL3 to the right side of region CL4 and may be caused by heating as significant quantities of gas from the filament plough into the main cluster. Thus the cooler region is detected towards the outer edge while the hotter region is detected at the center where merging events occur. Further clusters CL2 and CL4 are identified as the cool cores of clusters merging with the main body of MACS $J0717.5 + 3745$ (Ma et al. 2008, 2009).

A spatial comparison of the low frequency radio image and the X−ray brightness image is shown in Fig. 7. The '$Chair − shaped$' filament structure with flat spectrum ($\alpha_{0.235}^{0.61} = -0.92 to -1.5$) is well placed between the merging region of the 4 clusters where high temperature activities are detected (10.2 ± 2.4 keV, Ma et al. 2009). The merging events causes heating of the thermal plasma due to shock, which inturn re−accelerates the relativistic particles and amplifies the magnetic field. The radio halo with steep spectra of $\alpha_{0.235}^{0.61} = -0.85 to -2.3$ from the central region near the '$Chair − shaped$' filament structure towards the outer edge, traces the overall outer edge and cooler region of the cluster. A correlation between the radio halo integrated spectral index and the average X−ray gas temperature for a large sample of nearby radio halos has been derived recently by Giovannini et al. 2009. Hot clusters ($T > 10 keV$) show an average spectral index $= -1.1$ to -1.2 and cold clusters ($T \leq 8$ keV) show steep spectra (average spectral index $= -1.7$), according to the correlation derived by Giovannini et al. 2009, Venturi et al. 2013. The radio spectrum of present radio halo with $\alpha \sim -1.17$ derived from our low frequency observations further confirms the result that flatter spectra are present in high temperature merging clusters (Ma et al. 2009).

Further Venturi et al. 2013 based on the mass of the cluster derived that, the radio halos show different spectra depending on the energy release into particle re−acceleration during mergers. The trend of flatter spectra is seen in massive hot clusters

($T > 8$ keV) with halos, while moderately massive clusters ($T \sim 5 - 8 keV$) shows halos with both steep and flat spectra (Cassano et al. 2006, Cassano et al. 2010). Fig. 8, reports the distribution of spectral index ($\alpha_{1400MHz}^{235MHz}$) in radio−halo clusters versus the X−ray temperature, kT (keV) adapted from Venturi et al. (2013). The position of MACS $J0717.5 + 3745$ is shown by red point with kT$=10.2 \pm 2.4$ keV. Thus, it is the most distant massive cluster with radio halo showing spectra flatter than ~ 1 as compared to other hotter clusters suggesting its complex nature. MACS $J0717.5 + 3745$, being most flattest among the massive galaxy clusters, is an interesting candidate that provides an upper limit for our understanding of mass−spectral index correlation of giant radio halos in distant massive hotter clusters with multiple mergers.

4.2. Spectral index distribution within the halo

We further carried out spectral index analysis of specific regions CL2, CL3 and CL4 where halo emission is detected at radio wavelengths and 3 merging clusters are detected from optical observations (Limousin et al. 2012). Fig. 9, shows Chandra contours overlaid on radio spectral index map between 0.61 and 0.235 GHz. A variation in the spectral index distribution is clearly seen to be coincident with the dynamical state of the cluster derived from X−ray images. The spectral index ($\alpha_{0.235}^{0.61}$) map analysis for Region CL2 shows a variation of -1.3 towards the outer edge and gradually decreases to -1.65 towards the '$Chair−shaped$' filament. In the case of region CL3, the spectral index varies from -1.2 from the outer edge to -2.3 towards the '$Chair − shaped$' filament. For region CL4, the spectral index is -1.3 at the outer edge and -0.98 towards the '$Chair − shaped$' filament. Thus, from the overall spectral index distribution analysis, we found that steep spectrum region is co−spatial with the colder region within MACS $J0717.5 + 3745$ and in confirmation with Ma et al. 2009.

In addition to the above spectral steepening trend, the diffuse radio emission in the halo shows additional spectral steepness at lower frequencies (Fig. 3 $Top Panel$) with $\alpha_{0.235}^{0.61} = -1.17 \pm 0.37$ as compared to higher frequencies $\alpha_{1.42}^{0.61} = -1.04 \pm 0.13$. Such
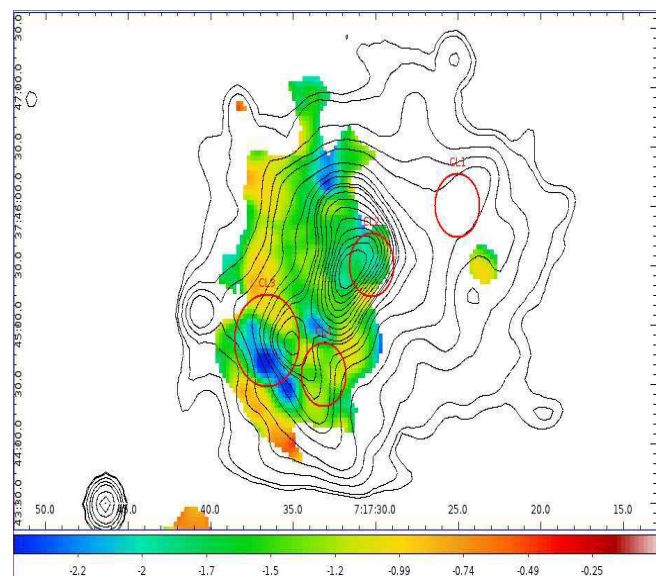

Fig. 9. MACS $J0717.5 + 3745$: GMRT spectral index map between 0.61 and 0.235 GHz with overlaid X−ray contours from *Chandra*.

upturn in the spectrum of the halo at lower frequencies have been measured in A2256 (Kale & Dwarakanath 2010, van Weeren et al. 2012). This trend of upturn in the spectrum could be due to superposition of at least two or more spectra having different steepness that adds up to flatten the spectra at low frequencies. In the case of MACS *J*0717.5 + 3745 the triple merger events could be the three epochs at which the electrons were accelerated with different input energy giving rise to varied spectral steepness. However, detailed simulations are required to establish the exact mechanism of acceleration of electrons to relativistic energies and the chronology between the three merger events. Typically the synchrotron spectrum is expected to steepen at higher frequencies due to energy losses. Thus putting together the spectral information across the frequency range of 0.235 to 4.86 GHz for the halo region, a scenario consistent with a high frequency steepening due to the energy losses and a low frequency flattening due to a secondary electron population emerges as seen in A2256 (Kale & Dwarakanath 2010, van Weeren et al. 2012).

An alternative scenario could be that the emission of the '*Chair − shaped*' filament could be projected on the halo emission causing a flattening of the spectrum at higher frequencies. The complex spectrum may simply result from a superposition of two components ('*Chair − shaped*' filament + halo). Further, the steeper spectral indices in the 1.42 − 4.86 GHz integrated spectra could be the act of ageing of the synchrotron spectrum due to energy losses. New observations with LOFAR at lower frequencies (< 0.235 GHz) and complementary observations at high frequencies are needed to determine the shape of the spectrum of the halo (cut−off), to better constrain its origin and image the entire extent of the diffuse bridge emission in the cluster at better sensitivity.

5. Conclusion

In this work we present a study of the radio emission in MACS *J*0717.5 + 3745 with more sensitive observation at 0.61 GHz and new map 0.235 GHz with the GMRT. We have confirmed the detection of the radio halo within the massive galaxy cluster down to 0.235 GHz. It is the most powerful and distant cluster ever observed. The results achieved from these observation are summarized below:

- A bright '*Chair − shaped*' filament structure is detected at 0.235 GHz at a linear scale of 853 kpc and at 0.61 GHz at 772 kpc. This '*Chair − shaped*' filament is enclosed in a diffuse halo structure of 1.6 kpc at 0.235 GHz and 1.5 kpc at 0.61 GHz. The complex morphology of the radio cluster indicates the ongoing merger activity within the cluster, supported by optical and X-ray studies.
- A radio power of 0.98×10^{-26}WHz^{-1} at 1.4 GHz is estimated from the steep radio spectral index of -1.17 derived from GMRT observations with a hint of steepening at lower frequencies.
- Using standard equipartition magnetic field assumption, we derived an equipartition magnetic field strength of 3.43 μG for the radio halo. A somewhat higher value of revised magnetic field strength of 6.49 μG is obtained by using lower and higher energy cutoffs instead of fixed frequency cutoffs.
- We also confirm the presence of additional diffuse bridge emission of ∼ 3.7 Mpc connecting the central radio halo with the discrete field source B and C, indicating the presence of magnetized ICM at this redshift.
- The location of the bright '*Chair − shaped*' filament coincides with regions in the cluster having higher temperatures.

The major axis of the '*Chair − shaped*' filament is located perpendicular to the merger axis of the system. This shows that the '*Chair − shaped*' filament is probably the result of a large−scale shock wave within the cluster where are particles are accelerated during merger events..

- In addition to the halo spectrum, we also analyzed the properties of the cluster discrete sources, specifically sources HT, B, C, C2, C4 and F. Sources HT and B are *head−tail* sources, while sources C, C2, C4 are unresolved and source F is extended with core and lobe morphology. The spectral index analysis along with NED counterparts suggests that these are radio galaxies with different origin of radio emission as compared to the cluster.

References

Bagchi M., Feretti, L., Giovannini, G., 2003, A&A, 400, 465
Beck, R., & Krause, M. 2005, Astron. Nachr., 326, 414
Becker, R. H., White, R. L., & Helfand, D. J. 1995, ApJ, 450, 559
Becker, R. H.; White, R. L., Helfand, D. J., Greeg, M. D., et al., 1994, AAS, 185
Bonafede, A., Feretti, L., Giovannini, G., et al. 2009a, A&A, 503, 707, 720
Bonafede, A., Giovannini, G., Feretti, L., Govoni, F., & Murgia, M. 2009b, A&A,494, 429
Boselli, A., & Gavazzi, G., 2006, PASP, 118, 517B
Briggs, D. S. 1995, PhD thesis, New Mexico Institute of Mining Technology, Socorro, New Mexico, USA
Brunetti, G., Setti, G., & Comastri, A. 1997, A&A, 325, 898
Brunetti, G., Setti, G., Feretti, L., & Giovannini, G. 2001, MNRAS, 320, 365
Brunetti, G., Giacintucci, S., Cassano, R., et al. 2008, Nature, 455, 944
Bruggen, M., van Weeren, R.J., Rottgering, HJA., 2011, Mem Soc Astron Ital, 82:627
Cassano, R., Brunetti, G., & Setti, G. 2006, MNRAS, 369, 1577
Cassano, R., Ettori, S., Giacintucci, S., et al. 2010b, ApJ, 721, L82
Chandra, P., Ray, A., & Bhatnagar, S. 2004, ApJ, 612, 974
Cohen, A. S., Lane, W. M., Cotton, W. D., et al. 2007, AJ, 134, 1245
Condon, J. J., Cotton, W. D., Greisen, E. W., Yin, Q. F., Perley, R. A., Taylor, G. B., & Broderick, J. J. 1998, AJ, 115, 1693
Cornwell, T. J., & Perley, R. A. 1992, A&A, 261, 353
Drury, L. O. 1983, Reports on Progress in Physics, 46, 973
Dursi, L. J., & Pfrommer, C. 2008, ApJ, 677, 993
Ebeling, H., Barrett, E., & Donovan, D. 2004, ApJ, 609, L49
Ebeling, H., Barrett, E., Donovan, D., et al. 2007, ApJ, 661, L33
Ensslin, T. A., Biermann, P. L., Klein, U., & Kohle, S. 1998, A&A, 332, 395
Ebeling, H., Edge, A. C., & Henry, J. P. 2001, ApJ, 553, 668
Edge, A. C., Ebeling, H., Bremer, M., et al. 2003, MNRAS, 339, 913
Fanaroff, B. L., & Riley, J. M. 1974, MNRAS, 167, 31P
Feretti, L. 2005, Advances in Space Research, 36, 729
Feretti, L. & Giovannini, G., 2008, Plionis M., L'opez-Cruz O, Hughes D (eds) Lect notes phys, vol 740, Springer, Dordrecht, p 143

Feretti, L., Giovannini, G., Govoni, F., Murgia, M., 2012, A&A, 20:54

Ferrari, C., Govoni, F., Schindler, S., Bykov, A. M., & Rephaeli, Y. 2008, SSRv,134, 93

Finoguenov, A., Sarazin CL, et al., 2010, Astrophys J, 715:1143

Giacintucci, S., Cassano, R., Brunetti, G., et al., 2013, to be submitted to ApJ (G12)

Giovannini, G., Bonafede, A., Feretti, L., et al. 2009, A&A, 507, 1257

Giovannini, G. & Feretti, L., 2004, J Korean Astron Soc 37:323

Govoni, F., Feretti, L., et al. 2004, IJMPD, 13, 1549

Govoni, F., Murgia, M., Feretti, L., et al. 2005, A&A, 430

Govoni, F., Murgia, M., et al. 2009, A&A, 430499, 371

Jaffe, W. J. & Perola, G. C. 1973, A&A, 26, 423

Kale, R. & Dwarakanath, K. S. 2009, ApJ, 699, 1883

Kale, R. & Dwarakanath, K. S. 2010, ApJ, 718, 939

Limousin, M.; Ebeling, H.; Richard, J.; Swinbank, A. M.; Smith, G. P.; et al., 2012, A&A, 544A, 71L

Ma, C.-J., Ebeling, H., Donovan, D.& Barrett, E. 2008, ApJ, 684, 160

Ma, C.-J., Ebeling, H., & Barrett, E. 2009, ApJ, 693, L56

Markevitch, M., Gonzalez, A. H., David, L., et al. 2002, ApJ, 567, L27

Markevitch, M., & Vikhlinin, A. 2007, Phys. Rep., 443, 1

Miniati, F., Jones, T. W., Kang, H., & Ryu, D. 2001, ApJ, 562, 233

Mroczkowski, Tony; Dicker, Simon; Sayers, Jack; Reese, Erik D.; Mason, Brian; Czakon, Nicole; Romero, Charles; et al., 2012, ApJ, 761, 47

Murgia, M., Eckert, D., Govoni, F., Ferrari, C., Pandey-Pommier, M., et al. 2009, A&A, 514, A76, 2010

Parrish, I. J., Quataert, E., & Sharma, P. 2009, ApJ, 703, 96

Perley, R. A. 1989, in Synthesis Imaging in Radio Astronomy, ed. R. A. Perley,F. R. Schwab, & A. H. Bridle, ASP Conf. Ser., 6, 259

Petrosian, V. 2001, ApJ, 557, 560

Rengelink, R. B., Tang, Y., de Bruyn, A. G., et al. 1997, A&AS, 124, 259

van Weeren, R., Rottgering, H. J. A., Bruggen, M. and Cohen, A., 2009, A&A, 505, 991, 997

van Weeren, R., Rottgering, H. J. A., Bruggen, M., et al., 2010, Science, 330, 347

van Weeren, R.,H. J. A. Rottgering, D. A. Rafferty, R. Pizzo, A. Bonafede, 2012, A&A, 543, 43

Venturi, T., Giacintucci, S., Brunetti, G., et al. 2007, A&A, 463, 937

Venturi, T., Giacintucci, S., Dallacasa, D., et al. 2008, A&A, 484, 327

Venturi, T.,Giacintucci, S., Dallacasa, D., et al., 2013, A&A

Zitrin, A., Broadhurst, T., Rephaeli, Y., Sadeh, S., 2009, ApJ, 707L, 102Z